The Journal of Engineering

IET International Radar Conference (IRC 2018)

IET Journals
The Institution of Engineering and Technology

Three-dimensional ISAR imaging: a review

eISSN 2051-3305
Received on 21st February 2019
Accepted on 20th May 2019
E-First on 20th September 2019
doi: 10.1049/joe.2019.0570
www.ietdl.org

Marco Martorella[1,2], Federica Salvetti[2] ✉, Daniele Staglianò[1], Elisa Giusti[2]

[1]*Department of Information Engineering, University of Pisa, Pisa, Italy*

[2]*Radar and Surveillance Systems (RaSS) National Laboratory, National Inter-university Consortium for Telecommunications (CNIT), Pisa, Italy*

✉ *E-mail: federica.salvetti@cnit.it*

Abstract: Three-dimensional (3D) inverse synthetic aperture radar (ISAR) imaging has been proven feasible by combining traditional ISAR imaging and interferometry. Such technique, namely inteferometric ISAR (In-ISAR), allows for the main target scattering centres to be mapped into a 3D spatial domain as point clouds. Specifically, the use of an In-ISAR system can overcome the main geometrical interpretation issues imposed by the monostatic acquisition geometry as the problem of cross-range scaling and unknown image projection plane (IPP). However, some issues remain such as scatterer scintillation, shadowing effects, poor SNR etc., which limit the effectiveness of 3D imaging. A solution to such unsolved issues can be found in the use of multiple 3D views, which can be obtained exploiting either multi-temporal or multi-perspective configurations or a combination of both. This study aims to review the main concepts to produce multi-view 3D ISAR images by using In-ISAR systems also presenting real data collected with a multi-static In-ISAR system.

1 Introduction

ISAR imaging has been deeply investigated in the last few decades as it provides some means for automatic target classification and recognition (ATC/ATR). Two-dimensional monostatic ISAR suffers from some critical issues. Among others, geometrical adverse conditions is a strong limitation to its effective use. In fact, if a target intentionally moves directly at the radar, no aspect angle variation is generated by the radar and consequently the 2D ISAR image cannot be formed. Bistatic ISAR allows to overcome this important issue. In addition, bistatic ISAR has counter-stealth capabilities as some targets are made stealthy against monostatic radars but they are detectable by bistatic radars. Therefore, bistatic radar imaging of stealthy targets may be possible. However, as for the monostatic geometry, bistatic radar imaging may be limited by the difficulty in the interpretation of a 2D ISAR image. In fact, 2D ISAR techniques generate a 2D image of the target, which represents a 2D projection of the true three-dimensional (3D) target reflectivity onto an image projection plane (IPP). The orientation of the IPP strongly depends on the radar-target geometry and on the target motions, which are typically unknown. The result is that the target projection onto the image plane cannot be predicted and the interpretation of the resulting ISAR images becomes complicated. Under these conditions, the projected two-dimensional image can only provide limited information and is often not sufficient for identifying and recognising the target. Also, another important issue is related to the shadowing effect due to the self-occlusion of parts of the target. Many advances have been recently made in the scientific radar community [1–6]. Specifically, the use of an interferometric ISAR (In-ISAR) system both in a monostatic and bistatic configuration has been recently proposed to generate a 3D point-like model of the target as to overcome the geometrical constraints and the interpretation issues [5, 7].

However, target scintillation and shadowing effects may compromise the 3D In-ISAR image formation. The first issue may be overcome by observing the target for sufficiently long time to form multiple 3D reconstructions. Such a collection of 3D reconstructions may be then jointly used to obtain a fused 3D reconstruction, which would appear more densely populated. On the other hand, the problem of shadowing may be mitigated with the use of a net of distributed radars where multiple 3D reconstructions can be obtained from quite different aspect angles. Both solutions necessitate however to combine data relative to different acquisition times or different sensors.

The state-of-the-art in the field of multi-static radar has recently moved forward through the introduction of an incoherent technique to join together multiple 3D In-ISAR reconstructions which can be obtained exploiting either multi-temporal or multi-perspective configurations or a combination of both [8–10]. This paper aims to review these recent advances of multi-view 3D In-ISAR imaging showing its versatility and potential.

The remainder of the paper is organised as follows: Section 2 briefly discusses the fundamentals of 3D In-ISAR imaging. Section 3 describes the concept of multi-view fusion and Section 4 shows a collection of results obtained by processing real data in different operating modes. Finally, Section 5 is dedicated to remarks and conclusion.

2 Concept of 3D In-ISAR imaging

In order to achieve 3D imaging, interferometric systems need to be formed by a number of receivers experiencing angle variation both in the azimuth and the elevation directions so to coherently combine the inter-element phase differences. Thus, a cost-effective solution is to use the minimum number of receivers, which is equal to three and are typically located onto two orthogonal baselines of size d_V and d_H as shown in Fig. 1.

The three receiving antennas (V,C,H) are positioned in the reference system T_ζ, which is embedded on the central receiver of the multichannel radar system. In a monostatic configuration, the transmitting antenna is co-located with a receiving antenna. A more general case includes a fourth transmitting antenna located at a meaning distance from the receiving antennas, that is, a bistatic geometry [11]. This geometry must be handled properly as bistatic angle changes during the CPI may cause ISAR image distortions. In [7, 12], the bistatic configuration is treated by adopting the bistatically equivalent monostatic (BEM) approximation.

The channels (V_{eq}, C_{eq}, H_{eq}) correspond to the equivalent monostatic triad of transceivers in the T_ξ reference system. Despite the fact that the baselines formed by the receivers are orthogonal, the ones formed by equivalent monostatic transceivers do not necessarily define two orthogonal equivalent baselines. The whole 3D In-ISAR imaging processing chain is described in [5, 7], where the received signal modelling, the multichannel ISAR image

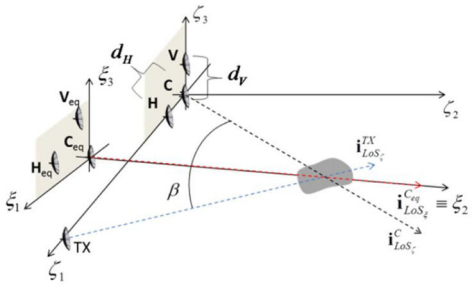

Fig. 1 *Multi-bistatic configuration*

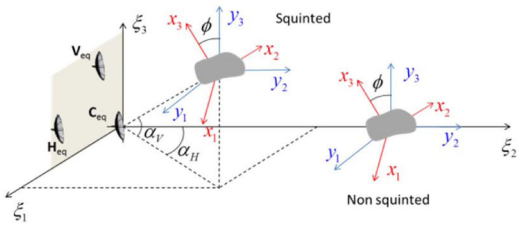

Fig. 2 *Multichannel configuration after BEM approximation*

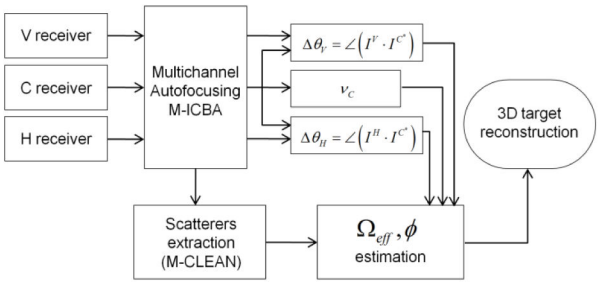

Fig. 3 *Overall flowchart of 3D reconstruction processing*

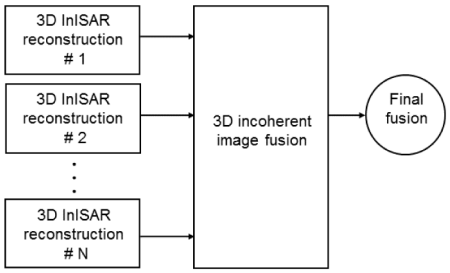

Fig. 4 *3D fusion algorithm's concept*

formation algorithm as well as the bistatic 3D In-ISAR reconstruction algorithm are detailed. The above-mentioned 3D In-ISAR method is based on the assumption that the line between the origin of the radar reference system and the target is orthogonal to the plane containing the antennas. Thus, when this condition is not met, a non-compensated residual phase cause errors in the height estimation of the scatterers and consequently the 3D reconstruction appear distorted. This case of a squinted configuration is addressed in [7] by using a post-processing technique to restore the non-squinted case condition. The geometry after BEM approximation is represented in Fig. 2.

The overall flowchart is depicted in Fig. 3, which is composed of the following steps: (1) multi-channel ISAR processing, (2) multi-channel scatterers extraction, and (3) scatterer height estimation.

Once the 2D ISAR images have been formed for each receiving channel, the brightest scatterers are extracted by means of the MC-CLEAN algorithm [5]. Then, for each scatterer that composes the target, the following information are extracted from the 2D ISAR images:

- The phase difference ΔV between the ISAR image relative to the vertical channel, V_{eq}, and the ISAR image relative to the central channel, C_{eq}.
- The phase difference, ΔH, between the ISAR image relative to the horizontal channel, H_{eq}, and the ISAR image relative to the central channel, C_{eq}.
- The Doppler frequency extracted from the ISAR image relative to central channel, ν_C.

Such information are linked with both the target effective rotation vector, $\mathbf{\Omega}_{\text{eff}}$, and the scatterer height y_3 by means of the following equations:

$$y_3 = \frac{cR_0}{4\pi f_0(d_H^z d_V^x - d_V^z d_H^x)} \cdot \tag{1}$$

$$\cdot \left[(d_V^x \Delta\theta_H - d_H^x \Delta\theta_V)\cos\phi - (d_H^z \Delta\theta_V - d_V^z \Delta\theta_H)\sin\phi\right]$$

$$\nu_C = \frac{R_0 \Omega_{\text{eff}}}{2\pi(d_H^z d_V^x - d_V^z d_H^x)} \cdot \tag{2}$$

$$\cdot \left[(\Delta\theta_H d_V^z - \Delta\theta_V d_H^z)\cos\phi - (\Delta\theta_V d_H^x - \Delta\theta_H d_V^x)\sin\phi\right]$$

where f_{O} is the operative frequency, d_V^x and d_V^z are the vertical channel components along ξ_1 and ξ_3, respectively, d_H^x and d_H^z are the horizontal channel components along ξ_1 and ξ_3, respectively. Furthermore, Ω_{eff} is the modulus of the target effective rotation vector and ϕ is the angle between $\mathbf{\Omega}_{\text{eff}}$ and the y_3-axis. Both y_3 and ϕ are jointly estimated from (2) by means of the least square error method by using the measured values within the position of the extracted scatterers. Once the angle ϕ is estimated, the scatterer height can be computed by using (1).

3 Multi-view 3D In-ISAR image fusion

Shadowing effects, scatterers scintillation, low SNR, and geometrically adverse cases may cause the monostatic 3D In-ISAR system to produce an incomplete or partial three-dimensional image of the target. An efficient solution to this problem is to incoherently join together multiple images of the same target in order to densely populate the 3D cloud of points representing the target's shape. The advantage of the incoherent method described in [8] is that images can be fused starting from those obtained either by using a net of spatially distributed radars, that is a multi-static system or a multi-temporal data set [9] or a combination of both [10], as depicted in Fig. 4.

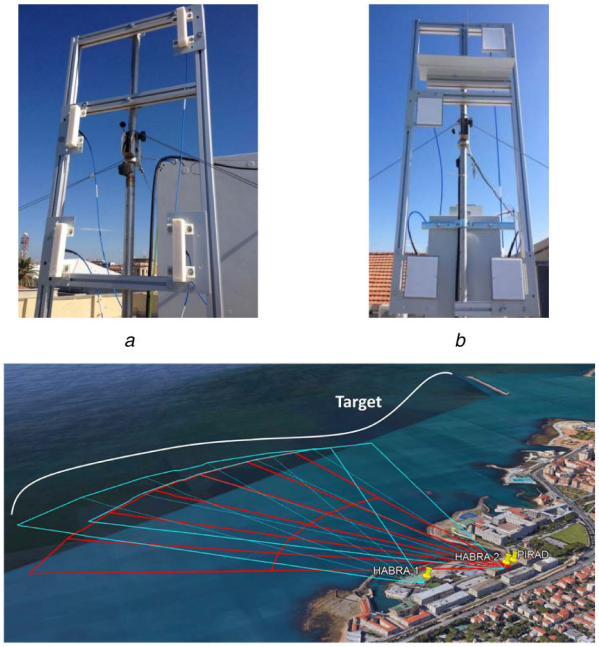

a b c

Fig. 5 *Livorno trials – radar systems and scenario*
(a) PIRAD, ***(b)*** HABRA, ***(c)*** Operative scenario

Length	33.25 m
Width	6.47 m
Height	15 m

Fig. 6 *Cooperative target — Training ship Astice*

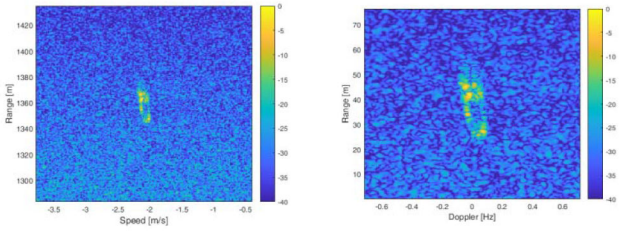

a b

Fig. 7 *Radar image of ASTICE before and after ISAR processing*
(a) Range-Doppler Map, ***(b)*** ISAR image

First, the 3D reconstructions are aligned to the same reference system. This is possible because an estimate of the orientation of the IPP of the specific radar-target acquisition scenario is obtained throughout the 3D In-ISAR processing. When more than two reconstructions need to be joined together, the 3D fusion algorithm runs iteratively by taking into account a pair of 3D images first. The reconstruction with the lowest number of scatterers N is labelled as the reference while the other is composed of M scattering points. Subsequently, the algorithm is repeated between the resulting fusion and another 3D reconstruction and so on. The main steps of the 3D fusion algorithm illustrated in Fig. 4 are described as follows and are applied to all the N scatterers:

- Identification of the possible matches by comparing to a threshold the height error between the nth scatterer of the reference and all the M scatterers of the other reconstruction. A match is declared when the height error is lower than the threshold.
- Alignment of the reference with the other reconstruction by overlapping all the matches and computation of the best alignment for the particular nth scatterer.

Once these steps are performed for all the N scatterers of the reference, the overall best alignment is decided based on the maximum number of common scatterers and on a reliability indicator named '*mean matching distance*' defined as the mean Euclidean distance between all the associated scatterers.

4 3D In-ISAR imaging in operative scenarios

In this section, results are collected to review the potential and show the versatility of the multi-view 3D In-ISAR imaging approach.

The measurement campaign was hosted in Livorno at the Institute 'G. Vallauri' in the Italian Navy Base in September–October 2014 during the NATO-SET 196 Joint Trials. During the trial, the interferometric multi-channel ISAR systems HABRA 1, HABRA 2, and PIRAD were deployed for monitoring the scenario from different aspect angles. The In-ISAR systems consist of one transmitting and three receiving elements arranged in an L-shape. Fig. 5 shows the systems and the operative scenario.

A number of cooperative targets have been used with the aim to better assess the algorithm performances. Results shown here refers to the cooperative target Astice, which is depicted in Fig. 6 along with its size.

4.1 Bistatic 3D In-ISAR

The RD map obtained in a bistatic case is shown in Fig. 7*a*. The ISAR image of the selected target after motion compensation is shown in Fig. 7*b*. Numerical results are reported in Table 1. The 3D reconstruction results are shown in Fig. 8. In particular, Fig. 8*a–c* represent a top, a side, and a front view of the target. As it is possible to see, the estimated sizes underestimate the actual ones. This might be due to some missed scatterers. In fact, because of shadowing effects, some scatterers may be lost in the 2D-ISAR images, thus affecting the interpretation of the reconstructed 3D target image. Such an issue can be mitigated by the multi-view processing as shown in next section.

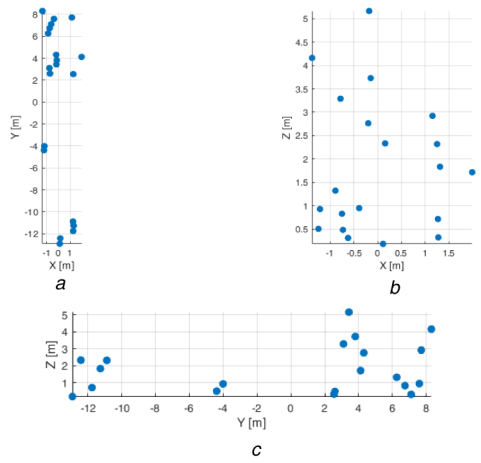

Fig. 8 *3D reconstruction (bistatic configuration)*
(a) (X–Y) plane, ***(b)*** (X–Z) plane, ***(c)*** (Y–Z) plane

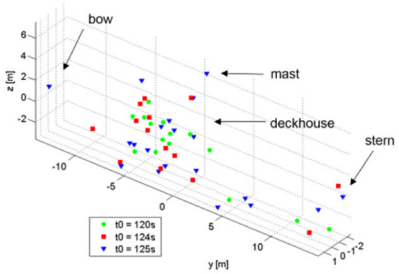

Fig. 9 *3D In-ISAR results relative to the three time intervals*

4.2 Multi-temporal3D In-ISAR

A cost-effective solution to obtain a more detailed 3D image of a target of interest is to use multi-temporal batches of received data acquired by a single interferometric sensor. Scintillation effects of the scattering centres generally cause 2D images of a multi-temporal sequence to show different scatterers. These images, collected during a short or a long temporal baseline, in turn generate different 3D reconstructions that can be incoherently joined together to increase information about the target.

4.2.1 Short temporal baseline: Several 3D target reconstructions can be obtained with a single interferometric sensor by collecting data from the target a different times. This allows for multiple 3D reconstruction to be fused into a more complete 3D reconstruction if the target's aspect angle is different from frame to frame. Due to scattering mechanism scintillation, a target observed from slightly different aspect angles may still show different sets of bright scatterers. This allows for different 3D reconstructions to be obtained even within relatively small time intervals. Fig. 9 shows three 3D In-ISAR reconstructions relative to the three time intervals and aligned to the same reference system. The multi-temporal data are acquired with the interferometric sensor PIRAD. The multi-temporal 3D image, superimposed with the CAD, is showed in Fig. 10.

4.2.2 Long temporal baseline: If a target does not change its characteristics in time, multiple 3D reconstruction may be obtained from data collected at very different times (days, weeks, months). Following up this concept, we may think of using this characteristic to update a database when another acquisition of the same target occurs. In an ATR scenario, a database should always be updated when possible. Therefore, when a target identification is confirmed, the same data used to identify the target can be used to update the database via a 3D fusion. Fig. 11 shows two 3D In-ISAR reconstructions relative to two different days of campaign and acquired by the same sensor PIRAD.

It is clear that the information about the target of interest highly increases when new 3D reconstructions are available (Table 2).

Table 1 Numerical results for trial with HABRA1 and HABRA2

R_0	1358 m
length	20.2 m
width	4.3 m
height	5.1 m
Ωeff	0.05 rad/s
ϕ	−4.93°
v_r	−2.1 m/s

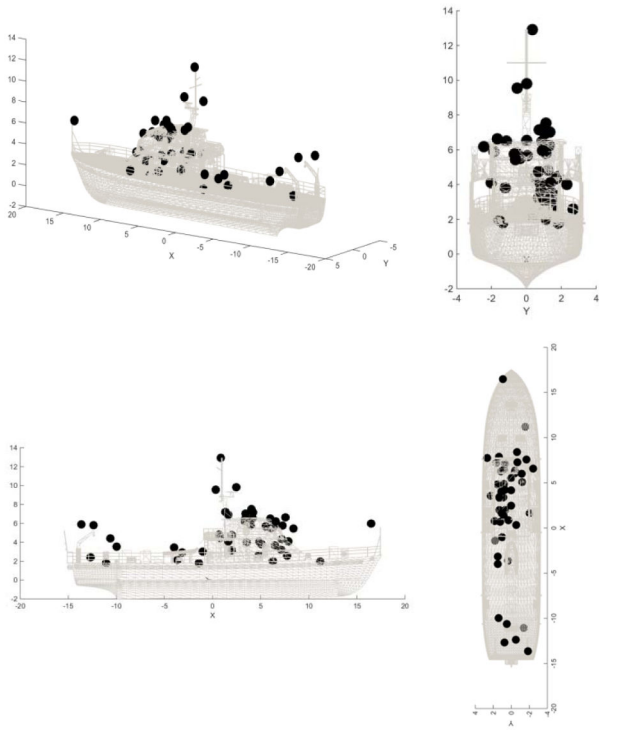

Fig. 10 *Multi-temporal 3D In-ISAR reconstruction – short temporal baseline*

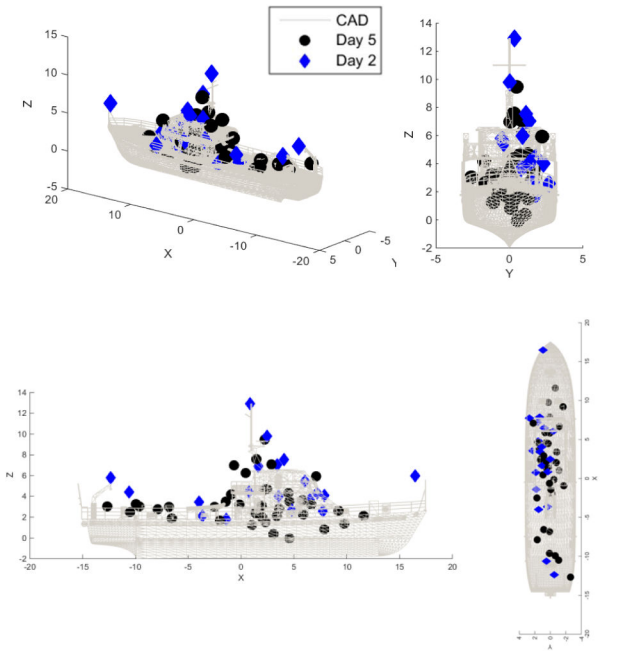

Fig. 11 *Multi-temporal 3D In-ISAR reconstruction – long temporal baseline*

Table 2 Estimated target's size. Multi-temporal-short temporal baseline

	Actual size	Multi-temporal reconstruction
length	32.4 m	30.1 m
width	6.47 m	5.1 m
height	12.5 m	11.1 m

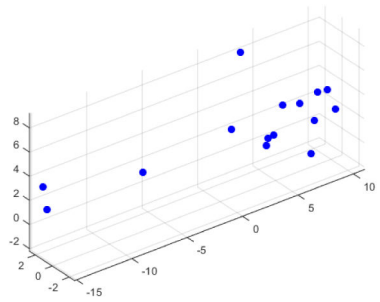

Fig. 12 *Monostatic 3D reconstruction – HABRA 1*

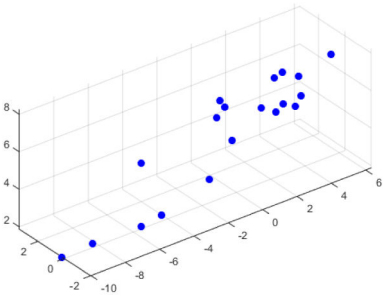

Fig. 13 *Monostatic 3D reconstruction – HABRA 2*

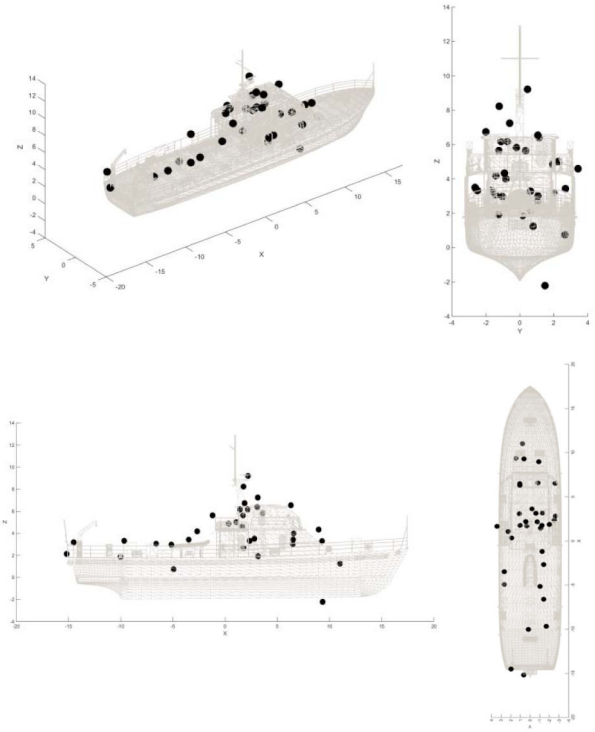

Fig. 14 *Multistatic 3D In-ISAR fusion*

4.3 Multi-static 3D In-ISAR

Multi-static 3D reconstruction may become available if multiple In-ISAR systems are in place. One of the main advantages of a multi-static configuration is that multiple 3D reconstructions can be simultaneously available for 3D fusion, therefore, reducing the time needed to obtain a satisfactory 3D reconstruction. Also, a number of sensors may be positioned strategically to defeat the problems of self-occlusion and stealthy targets.

Two 3D reconstructions of the training ship Astice have been obtained by using two interferemetric sensors, namely HABRA 1, HABRA2, in a multi-static configurations and shown in Figs. 12 and 13. HABRA 1 and HABRA 2 are illuminating the target simultaneously. The resulting 3D In-ISAR fusion is shown in Fig. 14, while Table 3 details the estimated size in comparison with the actual size of the target.

Table 3 Estimated target's size. Multi-static configuration

	Actual size	Multi-temporal reconstruction
length	32.4 m	25.3 m
width	6.47 m	6 m
height	12.5 m	11.4 m

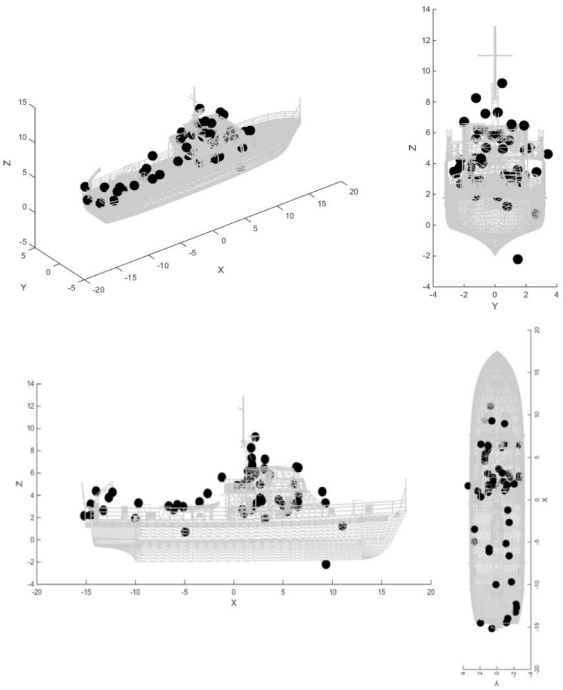

Fig. 15 *Multi-view 3D In-ISAR fusion*

4.4 Multi-view 3D In-ISAR

A combination of the above-mentioned set up can be used to increase information about the target, as shown in Fig. 15. Three 3D reconstructions of the training ship Astice have been obtained by using three interferemetric sensors, namely HABRA 1, HABRA2, and PIRAD. HABRA 1 and HABRA 2 are illuminating the target simultaneously while the reconstruction obtained with the PIRAD system results from processing data acquired in a different day and time.

5 Conclusion

This paper reviews the main concepts to produce multi-view 3D ISAR images by using In-ISAR systems and shows real data collected with a multi-static In-ISAR system in the framework of the NATO-SET 196 Joint Trials.

Results show that 3D In-ISAR imaging is an effective and reliable technique to form 3D images of a non-cooperative target. Moreover, the system's ability to reconstruct the 3D target's shape significantly increase when joining together multiple views. In fact, multi-view fusions result more densely populated and describe more accurately the target of interest. In addition, important target's features can be extracted with more consistency, paving the way to automatic target recognition and classification by using 3D reconstructions.

6 Acknowledgments

The authors would like to thank the Centro di Supporto e Sperimentazione Navale – Istituto per le Telecomunicazioni e l'Elettronica 'Giancarlo Vallauri' (CSSN-ITE), an experi- mental facility of the Italian Navy, for technical and logistic support given during the experiment that took place in Livorno. The authors would also to thanks the NATO for partially funding this work under the framework of The NATO Set 196 'Multichannel/ Multistatic Radar Imaging of Non-cooperative Targets'.

7 References

[1] Brisken, S., Worms, J.G.: 'ISAR motion parameter estimation via multilateration'. 2011 Microwaves, Radar And Remote Sensing Symp., Kiev, Ukraine, August 2011, pp. 190–194

[2] Brisken, S., Martorella, M., Mathy, T.*, et al.*: 'Motion estimation and imaging with a multistatic ISAR system', *IEEE Trans. Aerosp. Electron. Syst.*, 2014, **50**, pp. 1701–1714

[3] Battisti, N., Martorella, M.: 'Intereferometric phase and target motion estimation for accurate 3D reflectivity reconstruction in ISAR systems'. 2010 IEEE Radar Conf., Washington DC, USA, May 2010, pp. 108–112

[4] Wang, G., Xia, X.-G., Chen, V.C.: 'Three-dimensional ISAR imaging of maneuvering targets using three receivers', *IEEE Trans. Image Process.*, 2001, **10**, pp. 436–447

[5] Martorella, M., Staglianò, D., Salvetti, F.*, et al.*: '3D interfero-metric ISAR imaging of noncooperative targets', *IEEE Trans. Aerosp. Electron. Syst.*, 2014, **50**, pp. 3102–3114

[6] van Dorp, P., Otten, M.P.G., Verzeilberg, J.M.M.: 'Coherent multistatic ISAR imaging'. IET Int. Conf. on Radar Systems (Radar 2012), Glasgow, UK, October 2012, pp. 1–6

[7] Staglianò, D., Giusti, E., Lischi, S.*, et al.*: 'Bistatic three- dimensional interferometric ISAR', *IET Radar, Sonar Navig.*, 2016, **10**, (1), pp. 63–75

[8] Salvetti, F., Giusti, E., Staglianò, D.*, et al.*: 'Multistatic 3D ISAR image reconstruction'. 2015 IEEE Radar Conf. (RadarCon), Washington DC, USA, May 2015, pp. 0640–0645

[9] Giusti, E., Salvetti, F., Staglianò, D.*, et al.*: '3D InISAR imaging by using multi-temporal data'. Proc. of EUSAR 2016: 11th European Conf. on Synthetic Aperture Radar, Hamburg, Germany, June 2016, pp. 1–5

[10] Salvetti, F., Giusti, E., Staglianò, D.*, et al.*: 'Incoherent fusion of 3D InISAR images using multi-temporal and multi-static data'. 2016 IEEE Radar Conf. (RadarConf), Philadelphia, PA, USA, May 2016, pp. 1–6

[11] Martorella, M., Palmer, J., Homer, J.*, et al.*: 'On bistatic inverse synthetic aperture radar', *IEEE Trans. Aerosp. Electron. Syst.*, 2013, **43**, (3), pp. 1125–1134

[12] Martorella, M., Cataldo, D., Brisken, S.: 'Bistatically equivalent monostatic approximation for bistatic ISAR'. 2013 IEEE Radar Conf. (RADAR), Ottawa, Canada, 2013, pp. 1–5